Electroweak interactions in a relativistic Fermi gas

K. Vantournhout,* N. Jachowicz, and J. Ryckebusch
Department of Subatomic and Radiation Physics, Ghent University, Proeftuinstraat 86, B-9000 Gent, Belgium
(Dated: February 9, 2008)

We present a relativistic model for computing the neutrino mean free path in neutron matter. Thereby, neutron matter is described as a non-interacting Fermi gas in beta-equilibrium. We present results for the neutrino mean free path for temperatures from 0 up to 50 MeV and a broad range of neutrino energies. We show that relativistic effects cause a considerable enhancement of neutrino-scattering cross-sections in neutron matter. The influence of the Q^2-dependence in the electroweak form factors and the inclusion of a weak magnetic term in the hadron current is discussed. The weak-magnetic term in the hadron current is at the origin of some selective spin dependence for the nucleons which are subject to neutrino interactions.

PACS numbers: 25.30.Pt, 13.15.+g,26.60.+c,26.50.+x

I. INTRODUCTION

Neutrino interactions play a leading role in a variety of astrophysical phenomena. For example, neutrinos witnessed nuclear processes during the Big Bang, they became famous as messengers from our sun, and are recognized as the representatives from distant stars. Reaching us from the center of an exploding star, neutrinos are the first heralds announcing the end of the life of a massive star [1]. Their impact on the dynamics of a type-II supernova is crucial for the fate of the event. In the gravitational collapse of a massive star at the end of its life, an enormous amount of neutrinos is produced. During the last stages of the infall, the neutrinos are trapped inside the star's core. When the shock wave passes, densities in the star's center fall and the neutrinos become free to rush out, carrying away information about the structure of the proto neutron-star and about the supernova explosion mechanism [1]. For this, the basic mechanisms were established by the neutrinos observed from supernova 1987A. Theoretical simulations of core-collapse events [1], however, still face some major challenges. The shock wave tends to loose too much energy when traversing the iron core and no successful explosions can be reproduced. It has been suggested that the problems which the numerical simulations are facing, can be attributed to an incomplete description of the weak interaction processes involved [1]. An excellent knowledge about the cross sections for neutrino interactions with nuclei and nuclear matter over a wide range of densities and temperatures is of the utmost importance, hence constituting one of the major motivations for this work.

In recent years, the interactions of neutrinos with matter at supra-nuclear densities attracted a lot of attention. In most studies, approximations were made with respect to the description of the hadron gas (degrees of degeneracy, relativity, correlations) and the weak interaction (hadron current, relativistic effects). Tubbs and Schramm [2] pioneered calculations of the response of a hadron gas to electroweak fields. They investigated the extreme degenerate (or, quantummechanical) and completely non-degenerate (or, classical) limits of these processes for a non-interacting Fermi gas. Schinder [3] extended this work to all temperature and density conditions, thereby adopting an analytical technique based on the use of Fermi integrals. Several attempts have been made to implement the effect of correlations in the description of the hadron gas. Burrows and Lattimer [4] and Bruenn [5] included interactions in the Fermi gas using effective scaling factors. Ref. [6] extended these efforts to a microscopic description of interacting matter of arbitrary composition and degeneracy, in both non-relativistic and relativistic frameworks. Burrows and Sawyer [7] used correlation functions and Horowitz and Wehrberger [8] adopted a relativistic random phase approximation (RPA) approach. For all of the above-mentioned investigations, the weak interaction was modeled as a four-point Fermi-interaction with a four-momentum Q^2 independent hadron current thereby omitting weak magnetism. The weak magnetic contribution was shown to be non-negligible in Ref. [9]. Ref. [10] included the weak magnetic contributions within a non-relativistic RPA approach. Currently, new numerical techniques to investigate dense neutron matter are explored. Examples include studies based on molecular dynamics techniques [10, 11], describing the properties of the 'pasta' phases of nucleon matter and the correlated Tamm-Dancoff approximation (CDTA) [12].

In this paper we study lepton interactions with a non-interacting relativistic hadron gas, and pay special attention to relativistic mechanisms. In our approach nucleon matter is described in terms of a relativistic Fermi gas (RFG). This approach allows us to investigate the effect of relativistic kinematics on the phase-space in the interactions, and its influence on the cross sections. In con-

*Electronic address: Klaas.Vantournhout@UGent.be

trast to many previous studies, we retain the electroweak current in its full complexity and introduce Q^2-dependent electroweak form factors.

The outline of the paper is as follows. Section II sketches the RFG framework which we adopt. Section III presents the main ingredients of cross-section calculations for weak interactions between a neutrino and a nucleon gas. After testing the reliability of the relativistic formalism and the adopted numerical techniques in sections IV A and IV B, relativistic cross-section results are presented and discussed in sections IV C and IV D.

II. TWO-BODY SCATTERING IN A RELATIVISTIC FERMI GAS

We consider processes in which a particle a is impinging on a particle b, embedded in a gas. The differential cross section for the collision of the two particles resulting in the creation of N reaction products $a+b \to \sum_{f=1}^{N} x_f$ is given by

$$d^{3N}\sigma = \frac{(2\pi)^{10}}{v_{rel}} \prod_f d^3\vec{p}_f \delta^4(p_a + p_b - \sum_f p_f) \times |M(a+b \to \{f\})|^2 , \quad (1)$$

where p_a and p_b are the four-momenta of the colliding particles and the N outgoing particles f have four-momentum p_f. In a relativistic description, energy and momentum conservation are imposed through the four-dimensional Dirac delta function $\delta^4(p_a+p_b-\sum_f p_f)$. The dynamics of the interaction is described by the transition matrix element $M(a+b \to \{f\})$. The relative velocity v_{rel} represents the flux of incident particles. The general Lorentz-covariant formulation of this quantity is given by

$$v_{rel} = \frac{\sqrt{(p_a p_b)^2 - p_a^2 p_b^2}}{p_a^0 p_b^0} . \quad (2)$$

For head-on collisions, Eq. (2) reduces to the familiar expression

$$v_{rel} = \left| \frac{\vec{p}_a}{p_a^0} - \frac{\vec{p}_b}{p_b^0} \right| . \quad (3)$$

The gas of particles b on which the particles a are impinging is modeled in terms of the probability distribution $F^b_{\alpha_b}(\vec{r}_b, \vec{p}_b)$, describing the probability that a target particle b with quantum numbers α_b occupies a phase-space volume $d^3\vec{r}_b d^3\vec{p}_b$. For a homogeneous and non-interacting gas, the probability distributions are independent of $\vec{r}_b$: $F^b_{\alpha_b}(\vec{r}_b, \vec{p}_b) = F^b_{\alpha_b}(\vec{p}_b)$. For fermions, the cross section of Eq. (1) can be cast in the form

$$\mathcal{N} d^{3N}\bar{\sigma} = \sum_{\substack{\alpha_a, \alpha_b, \\ \{\alpha_f\}}} \int F^b_{\alpha_b}(\vec{p}_b) d^3\vec{p}_b \frac{(2\pi)^{10}}{v_{rel}} \prod_f F'^f_{\alpha_f}(\vec{p}_f) d^3\vec{p}_f \delta^4(p_a + p_b - \sum_f p_f) \left| M(a+b \to \{f\}) \right|^2 . \quad (4)$$

Here, $d^{3N}\bar{\sigma}$ represents the differential cross section per particle b, $F'^f_{\alpha_f}(\vec{p}_f)$ is the probability that the final state determined by (p_f, α_f) is unoccupied

$$F'^{x_f}_{\alpha_f}(\vec{p}_f) = 1 - F^{x_f}_{\alpha_f}(\vec{p}_f) . \quad (5)$$

Further, $\mathcal{N}$ is proportional to the number density of the gas

$$\mathcal{N} = \sum_{\alpha_b} \int F^b_{\alpha_b}(\vec{p}_b) d^3\vec{p}_b ,$$

where $\sum_{\alpha_b}$ represents the sum over all relevant quantum numbers. For an interaction of the type $a+b \to x+y$, the differential cross section per target particle b can be cast in the form

$$\mathcal{N} \frac{d^3\bar{\sigma}}{d|\vec{p}_x| d^2\Omega_x} = \sum_{\substack{\alpha_a, \alpha_b, \\ \alpha_x, \alpha_y}} \int F^b_{\alpha_b}(\vec{p}_b) d^3\vec{p}_b \frac{(2\pi)^{10}}{v_{rel}} \int F'^y_{\alpha_y}(\vec{p}_y) d^3\vec{p}_y \times \delta^4(p_a + p_b - p_x - p_y) \left| M(a+b \to x+y) \right|^2 F'^x_{\alpha_x}(\vec{p}_x) |\vec{p}_x|^2 , \quad (6)$$

where it was assumed that both x and y are embedded in a Fermi gas.

For the reaction $a + b \to x + y$ only a limited region in phase-space is accessible for the outgoing particles x and y. At the same time, an outgoing particle x with a four-momentum p_x, can only be created from a well-defined part of the initial phase space. The kinematic restrictions governing the interaction are dictated by four-momentum conservation. Defining the four-momentum difference $w = p_a - p_x$ and $W^2 = m_y^2 - m_b^2 - w^2$, it becomes straightforward to simplify the integral in Eq. (6). When the labels a and x are assigned to the incoming and outgoing lepton, the four-momentum difference w represents the four-momentum exchange q. For $|\vec{w}| \neq 0$, Eq. (6) can be cast in the form

$$\mathcal{N}\frac{d^3\bar{\sigma}}{d|\vec{p}_x|d^2\Omega_x} = \frac{1}{|\vec{w}|}\sum_{\substack{\alpha_a,\alpha_b,\\ \alpha_x,\alpha_y}}\int_{p_b^{MIN}}^{p_b^{MAX}}|\vec{p}_b|d|\vec{p}_b|\int_0^{2\pi}d\phi_b F^b_{\alpha_b}(\vec{p}_b)F'^y_{\alpha_y}(\vec{w}+\vec{p}_b)(w^0+p_b^0)\Theta(w^0+p_b^0-m_y)$$
$$\times\frac{(2\pi)^{10}}{v_{rel}}\left|M(a+b\to x+y)\right|^2 F'^x_{\alpha_x}(\vec{p}_x)|\vec{p}_x|^2,$$

in which the condition

$$\cos\theta_{\vec{w},\vec{p}_b} = \frac{-W^2+2w^0p_b^0}{2|\vec{w}||\vec{p}_b|} = \frac{-W^2+2w_0\sqrt{m_b^2+|\vec{p}_b|^2}}{2|\vec{w}||\vec{p}_b|}, \tag{7}$$

must be obeyed. The integration limits for the initial momentum $|\vec{p}_b|$ are the solutions of $\cos\theta_{\vec{w},\vec{p}_b} = \pm 1$ and are listed in Table I.

For the peculiar situation that $|\vec{w}| = 0$, Eq. (6) becomes

$$\mathcal{N}\frac{d^3\bar{\sigma}}{d|\vec{p}_x|d^2\Omega_x} = \left|\frac{-W^2}{w_0\sqrt{W^4-4w_0^2m_b^2}}\right|\sum_{\substack{\alpha_a,\alpha_b,\\ \alpha_x,\alpha_y}}\iint_{4\pi}d^2\Omega_b F^b_{\alpha_b}(\vec{p}_b)F'^y_{\alpha_y}(\vec{p}_b)(w^0+p_b^0)\Theta(w^0+p_b^0-m_y)$$
$$\times\frac{(2\pi)^{10}}{v_{rel}}\left|M(a+b\to x+y)\right|^2 F'^x_{\alpha_x}(\vec{p}_x)|\vec{p}_x|^2|\vec{p}_b|^2, \tag{8}$$

with

$$|\vec{p}_b| = \sqrt{\frac{W^4}{4w_0^2}-m_b^2}\,. \tag{9}$$

Nucleon matter at supra-nuclear densities can be described as a partially degenerate Fermi gas. In the remainder of this paper, the probability distributions $F^i_{\alpha_i}$ are replaced by Fermi distributions

$$F^i_{\alpha_i}(\vec{p}) = \frac{1}{\exp\left(\dfrac{E_i(\vec{p})-\mu_i}{kT}\right)+1}. \tag{10}$$

The introduction of this probability distribution violates the Lorentz invariance of Eq. (6).

We deal with a mixture of a proton, neutron, electron and neutrino gas. In an equilibrium situation, the second law of thermodynamics imposes relations between their respective chemical potentials. For reactions of the type

$$\nu_e + n \leftrightarrow e^- + p, \tag{11}$$

the sum of the chemical potentials of the initial and final states should be equal. Considering that the total system is neutral and denoting the baryon density by n_B, beta-equilibrium requires that the following conditions are obeyed :

$$\mu_{\nu_e} + \mu_n = \mu_{e^-} + \mu_p, \tag{12a}$$
$$n_p = n_{e^-}, \tag{12b}$$
$$n_p + n_n = n_B. \tag{12c}$$

A fourth condition is related to neutrino trapping. In the absence of trapping one has

$$\mu_{\nu_e} = 0\,. \tag{12d}$$

TABLE I: Overview of the integration limits for $|\vec{p}_b|$.

	p_b^{MIN}	p_b^{MAX}
$w^2 < 0$	$\frac{1}{2}\left\lvert\frac{W^2\lvert\vec{w}\rvert}{w^2} + w_0\sqrt{\frac{W^4}{w^4} - \frac{4m_b^2}{w^2}}\right\rvert$	∞
$w^2 < 0, W^4 = 4w^2m_b^2$	no solution	
$w^2 < 0, W^2 = 2w_0m_b$	0	∞
$w^2 = 0$	$\left\lvert\frac{\lvert\vec{w}\rvert m_b^2}{W^2} - \frac{W^2}{4\lvert\vec{w}\rvert}\right\rvert$	∞
$w^2 > 0, W^4 > 4w^2m_b^2$	$\frac{1}{2}\left\lvert\left\lvert\frac{W^2\lvert\vec{w}\rvert}{w^2}\right\rvert - \lvert w_0\rvert\sqrt{\frac{W^4}{w^4} - \frac{4m_b^2}{w^2}}\right\rvert$	$\frac{1}{2}\left\lvert\left\lvert\frac{W^2\lvert\vec{w}\rvert}{w^2}\right\rvert + \lvert w_0\rvert\sqrt{\frac{W^4}{w^4} - \frac{4m_b^2}{w^2}}\right\rvert$
$w^2 > 0, W^4 \leq 4w^2m_b^2$	no solution	
$w^2 > 0, W^4 = 4w_0^2m_b^2$	0	$\left\lvert\frac{W^2\lvert\vec{w}\rvert}{w^2}\right\rvert$

When trapping occurs one defines

$$\frac{n_{e^-} + n_{\nu_e}}{n_B} = Y_\ell. \tag{12e}$$

Common values for Y_ℓ are in the range between 0.3 and 0.4 [13]. For fermions, the number density n_i is determined from

$$n_i = \frac{1}{2\pi^2}\int_0^\infty \frac{p^2}{\exp\left(\frac{\sqrt{p^2+M_i^2}-\mu_i}{kT}\right)+1}dp\,. \tag{13}$$

III. ELECTROWEAK INTERACTION MATRIX ELEMENTS

In first-order perturbation theory, electroweak interactions between leptons and hadronic matter are described as the four-product of a lepton $\jmath_\mu$ and hadron current J_ν, a tensor $B^{\mu\nu}$ representing the exchanged boson mediator, and a strength factor χ. We define p (P) and k (K) as the four momentum of the initial (final) lepton and hadron, q as the four-momentum exchange, Q^2 equals $-q_\mu q^\mu$. The chiralities of the initial and final leptons are denoted by λ and Λ. Further, s and S are the spins of the initial and final hadrons. The transition matrix element takes on the general form

$$iM\left(p\lambda + ks \to P\Lambda + KS\right) = \chi \jmath_\mu B^{\mu\nu} J_\nu, \tag{14}$$

and for neutral current (NC) reactions one has

$$\jmath_\mu B^{\mu\nu} J_\nu = -i\frac{G_F}{\sqrt{2}} M_Z \langle P;\Lambda|j_\mu^{NC}|p;\lambda\rangle \frac{g^{\mu\nu} - \frac{q^\mu q^\nu}{M_Z^2}}{M_Z^2 + Q^2}\langle K;S|J_\nu^{NC}|k;s\rangle, \tag{15}$$

for charged current (CC) reactions

$$\jmath_\mu B^{\mu\nu} J_\nu = -i\frac{G_F\cos\theta_C}{\sqrt{2}} M_W \langle P;\Lambda|j_\mu^{CC}|p;\lambda\rangle \frac{g^{\mu\nu} - \frac{q^\mu q^\nu}{M_W^2}}{M_W^2 + Q^2}\langle K;S|J_\nu^{CC}|k;s\rangle\,. \tag{16}$$

In the matrix element for charged-current interactions an extra factor $\cos\theta_C$ appears. This is due to the fact that the weak left-handed d-quark is an admixture of the strong left-handed d and s quarks. As a consequence, strangeness-conserving hadronic charged-current processes are weaker than their lepton counterparts.

The lepton weak neutral current is generally written as

$$\langle P;\Lambda|j_\mu^{NC}|p;\lambda\rangle = 4\langle P;\Lambda|\bar{\psi}\gamma_\mu(I_z^W - \sin^2\theta_W Q)\psi|p;\lambda\rangle\,, \tag{17}$$

where I_z^W represents the weak isospin operator, Q the charge operator and ψ are the normalized Dirac field operators.

For neutrinos the currents are given by

$$\langle P;\Lambda|j_\mu^{CC}|p;\lambda\rangle = \langle P;\Lambda|\bar{\psi}(1-\gamma_5)\gamma_\mu\psi|p;\lambda\rangle,$$

where the projection operator $(1-\gamma_5)$ takes into account that only left-handed neutrinos couple to the weak interaction. The final lepton ℓ is a massive lepton ℓ^- in CC reactions and a neutrino ν_ℓ for NC scattering processes.

The weak nucleon current is given by [14]

$$J_\nu = F_1(Q^2)\gamma_\nu + \frac{i}{2M_N}F_2(Q^2)\sigma_{\nu\mu}q^\mu + G_A(Q^2)\gamma_\nu\gamma_5 + \frac{1}{2M_N}G_P(Q^2)q_\nu\gamma_5, \quad (18)$$

where second-class currents were not considered. $F_1(Q^2)$ and $F_2(Q^2)$ are the Dirac form factors which are related to the well-known weak-electric and weak-magnetic form-factors through the relations $G_E = F_1 - \tau F_2$ and $G_M = F_1 + F_2$ where $\tau = Q^2/4M_N^2$. The Q^2-dependence of the weak Sachs vector form factors G_E and G_M is given by the dipole parametrization:

$$G(Q^2) = G(0)\left(1 - \frac{Q^2}{M_V^2}\right)^{-2}, \qquad M_V^2 = 710649 \text{ MeV}^2 \quad (19a)$$

$$G_E^0(0) = \left(\frac{1}{2} - \sin^2\theta_W\right)\tau_3 - \sin^2\theta_W, \qquad G_E^\pm(0) = 1 \quad (19b)$$

$$G_M^0(0) = \left(\frac{1}{2} - \sin^2\theta_W\right)(\mu_p - \mu_n)\tau_3 - \sin^2\theta_W(\mu_p + \mu_n), \qquad G_M^\pm(0) = (\mu_p + \mu_n) \quad (19c)$$

where $\sin^2\theta_W = 0.2312$, μ_p and μ_n are the proton and neutron magnetic moments and τ_3 is the isospin operator. The axial form factor is given by

$$G_A^\pm(Q^2) = -g_a\left(1 - \frac{Q^2}{M_a^2}\right)^{-2}, \qquad G_A^0(Q^2) = -\frac{g_a}{2}\left(1 - \frac{Q^2}{M_a^2}\right)^{-2} \quad (19d)$$

$$g_a = 1.262, \qquad M_a^2 = 1065024 \text{ MeV}^2. \quad (19e)$$

The pseudoscalar form factor is related to the axial one through the Goldberger-Treiman relation

$$G_P(Q^2) = -\frac{4M^2 G_A(Q^2)}{Q^2 + m_\pi^2}. \quad (20)$$

As q_μ can be written in terms of the lepton masses, the pseudoscalar contribution vanishes for neutral-current processes.

IV. RESULTS

Before presenting the numerical results of the cross-section calculations for neutrino interactions with nucleon matter in sections IV C and IV D, we establish the reliability of our formalism and the adopted numerical techniques. To this end, we study some well-defined limits for which our predictions can be compared with results from alternative approaches.

A. Neutrino scattering on a single nucleon

In former studies of the neutrino-nucleon and neutrino-nucleus response, a variety of expressions for the hadron currents has been used :

$$J_\nu^{V-A} = (1-\gamma_5)\gamma_\nu, \quad (21)$$

$$J_\nu^{RN} = (c_v - c_a\gamma_5)\gamma_\nu, \quad (22)$$

$$J_\nu^{Mag} = F_1(0)\gamma_\nu + \frac{i}{2M_N}F_2(0)\sigma_{\nu\mu}q^\mu + G_A(0)\gamma_\nu\gamma_5 + \frac{1}{2M_N}G_P(0)q_\nu\gamma_5, \quad (23)$$

$$J_\nu^{Q^2} = F_1(Q^2)\gamma_\nu + \frac{i}{2M_N}F_2(Q^2)\sigma_{\nu\mu}q^\mu + G_A(Q^2)\gamma_\nu\gamma_5 + \frac{1}{2M_N}G_P(Q^2)q_\nu\gamma_5 \quad (24)$$

The operator J_ν^{V-A} of Eq. (21) assumes that hadrons are point-like particles, with the weak interaction occurring on the hadron instead of on the quark level. With this hadron current, an approximation for the neutrino-nucleon cross section was derived in Ref. [2] :

$$\sigma^{T-Schr}(\epsilon) = \frac{1}{4}\frac{4G_F^2 m_e^2\hbar^2}{\pi c^2}\left(\frac{\epsilon}{m_e}\right)^2. \quad (25)$$

This expression is valid when the incoming neutrino-energy is sufficiently small in comparison with the nucleon mass $\epsilon \ll M_N$. The validity of this approximation can be appreciated from Fig. 1, when comparing the

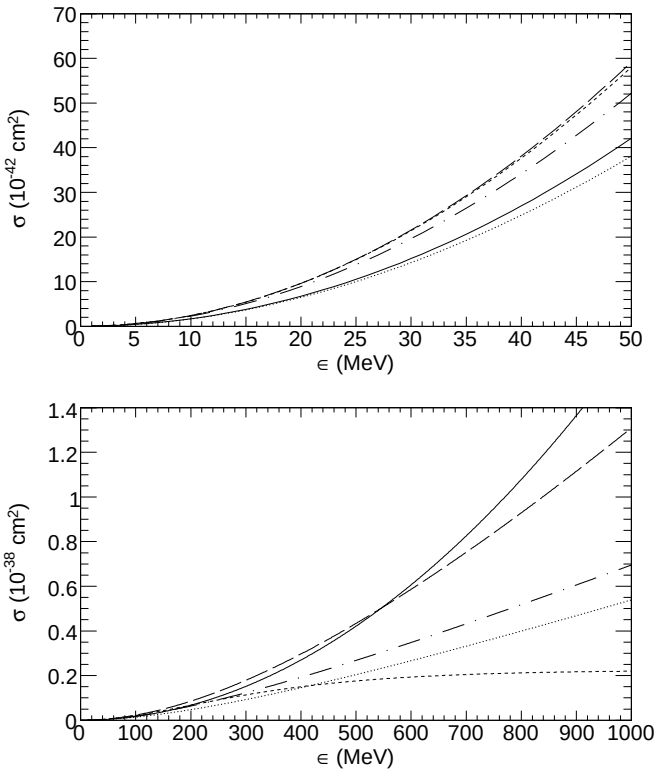

FIG. 1: The neutrino-neutron cross sections as a function of the incoming neutrino energy ϵ as obtained with different expressions for the nucleon current. The solid line refers to the analytical approximation of the cross section according to Eq. (25) ; the dotted line to cross sections obtained using the V-A current of Eq. (21) ; the renormalization effects of Eq. (22) are additionally taken into account in the dash-dotted curve. The long-dashed line corresponds to the cross sections for the current operator of Eq. (23) where the weak-magnetic contribution was added. The Q^2-dependence of the form factors shown in Eq. (24) is taken into account in the short-dashed curve.

solid line, representing the approximation (25), and the dotted line representing the cross section calculated with the current (21). From the top panel it emerges that the analytical expression of Eq. (25) is fine at low energies. From the results in the lower panel it is clearly seen that the approximation (25) is not valid any more at higher neutrino energies. The current operator J_ν^{RN} of Eq. (22) introduces renormalization effects that can be attributed to the strong interaction and the quark structure of the hadron. In the expression J_ν^{Mag}, the weak magnetic and pseudo-scalar contributions are added. The pseudo-scalar term vanishes for neutral-current processes. Due to its dependence on the momentum transfer, the contribution of the magnetic term is small at low energies. The operator $J_\nu^{Q^2}$ exhibits a Q^2-dependence in the form factors and can be interpreted as the most accurate expression for the hadronic weak current to date.

For each of the above current operators we display the computed neutrino-neutron cross section in Fig. 1. Thereby, we discriminate between low neutrino energies (up to 50 MeV) and neutrino energies that go up to the nucleon mass. At small incoming neutrino energies, our numerical results are in good agreement with the analytical expression of Eq. (25). With increasing neutrino energies, the deviation between the expression Eq. (25) and results obtained with more sophisticated current operators grows. The magnetic contribution in the current operator considerably enhances the cross sections at higher energies, while the introduction of Q^2-dependent form factors reduces the cross section strongly at large incoming neutrino energies.

B. Neutrino interactions with a neutron gas in the ($T = 0$ K, $\mu = M_n$ MeV) limit

When the value of the chemical potential μ approaches the rest mass of a free nucleon, or $\tilde{\mu} = \mu - M_n$ approaches zero and the temperature comes close to $T = 0$ K, neutrino-scattering cross sections in the neutron gas are expected to approach those of neutrino interactions on a single neutron in its rest frame. Indeed, at $T = 0$ K a decrease of the chemical potential implies a reduction of the average kinetic energy. At $\mu = M_n$, the kinetic energy vanishes. Hence, this limit of the Fermi-gas calculation provides a stringent test of the formalism and of the adopted numerical techniques. The results of this comparison between Fermi-gas and free-neutron cross sections, are presented in Fig. 2. When turning off the effect of the chemical potential ($\tilde{\mu} \to 0$), the influence of the other particles on the struck nucleon diminishes, a process which results in growing cross sections. The figure demonstrates that in the limit of vanishing chemical potential the cross sections computed in the hadron gas coincide with those on a single nucleon. The right panel of Fig. 2 shows the temperature dependence of the RFG prediction at chemical potentials approaching the rest mass of the hadrons. The numerical calculations were performed for $\tilde{\mu} = 1$ MeV. Again, the results converge to the single-nucleon cross-sections in the $T = 0$ K limit. This observation provides convincing evidence for the reliability of the adopted theoretical framework.

C. Relativistic effects in the phase-space factor

First, we investigate the role of relativistic effects in the phase-space factor. To this end, it is illustrative to introduce

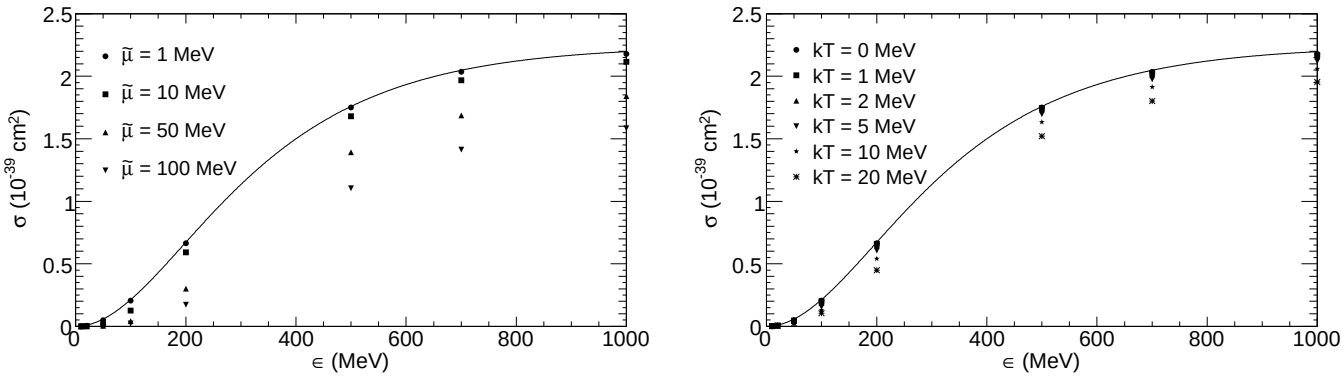

FIG. 2: Comparison between neutral-current cross sections on a single nucleon (solid line) and in a Fermi gas (markers). The left panel displays results for different values of the chemical potential and $T = 0$ K. In the right panel the temperature dependence is investigated for a chemical potential of $\tilde{\mu} = 1$ MeV. The chemical potentials are corrected for the rest mass of the free neutron.

$$\frac{d^3\Phi}{d|\vec{p}_x|d^2\Omega_x} = \sum_{\substack{\alpha_a,\alpha_b,\\ \alpha_x,\alpha_y}} \int F^b_{\alpha_b}(\vec{p}_b)d^3\vec{p}_b \int F'^y_{\alpha_y}(\vec{p}_y)\, d^3\vec{p}_y \delta^4(p_a + p_b - p_x - p_y) F'^x_{\alpha_x}(\vec{p}_x)|\vec{p}_x|^2 \,. \tag{26}$$

This quantity is independent of the dynamics of the $a+b \rightarrow x+y$ reaction. Even at low neutrino energies, sizable differences between relativistic and non-relativistic expressions for the phase-space integral emerge. In order to quantify this, we compare the dynamic form factor $S(\omega, |\vec{q}|)$ of the non-relativistic calculation of Ref. [6] with our relativistic one. Defining $w = q = p_a - p_x$ and assuming that $m_y = m_b$, Eq. (26) can be cast in the following form

$$\frac{d^3\Phi}{d|\vec{p}_x|d^2\Omega_x} = F'^x_{\alpha_x}(\vec{p}_x)|\vec{p}_x|^2 S(\omega, |\vec{q}|). \tag{27}$$

As shown in Ref. [6], in the non-relativistic limit this equation has an analytical solution. For completeness we wish to mention that even in the relativistic situation a solution for $S(\omega, |\vec{q}|)$ in terms of polylogarithmic functions can be found in Ref. [15]. From Fig. 3, it is clear that above a certain momenta, the relativistic Fermi distribution F_R is larger than its non-relativistic counterpart F_{NR}. In general,

$$\int_{p_-}^{\infty} F_R(p)p^2dp \geq \int_{p_-}^{\infty} F_{NR}(p)p^2dp. \tag{28}$$

As can be appreciated from Fig. 4, this relation ensures that $S(\omega, |\vec{q}|)$ is larger when computed in a relativistic approach. At moderate momentum transfers, the effect of relativity is limited to affecting the absolute magnitude of $S(\omega, |\vec{q}|)$. At higher $|\vec{q}|$-values, an additional effect in the ω dependence of $S(\omega, |\vec{q}|)$ appears. The shift towards lower values of ω is related to the differences in the lower limit of the integration over $|\vec{p}_b|$ in $S(\omega, |\vec{q}|)$. For higher momentum exchange, the term $F'^y_{\alpha_y}(\vec{q} + \vec{p}_b)$ in Eq. (26) approaches one. Hence the influence of the momentum distribution of the gas $F^b_{\alpha_b}(\vec{p}_b)$ becomes prominent, causing $S(\omega, |\vec{q}|)$ to reach a maximum at $p_b^{MIN} = 0$. Relativistically, the corresponding value for the energy exchange ω is given by $q^2/(m_b + \sqrt{m_b^2 + q^2})$, while in a non-relativistic calculation this quantity equals $q^2/(2m_b)$.

The role of relativity in the dynamical form factor $S(\omega, |\vec{q}|)$ can be easily estimated in the non-degenerate limit. Indeed, the classical limit will be reached when $(\mu_i - M)/kT \ll 0$. Under those conditions, one obtains the following closed relativistic form for $S(\omega, |\vec{q}|)$

$$S(\omega, |\vec{q}|) = \frac{2\pi}{|\vec{q}|} kT \left[\omega(m_b + kT + T_-) + (m_b + kT + T_-)^2 + (kT)^2\right] \exp\left(\frac{\mu_b - E_-}{kT}\right) \,, \tag{29}$$

where the following quantities were introduced,

$$E_- = \sqrt{p_b^{MIN^2} + m_b^2}, \qquad T_- = E_- - m_b, \tag{30}$$

A non-relativistic approach leads to a closed expression with only one term [6]

$$S(\omega, |\vec{q}|) = \frac{2\pi}{|\vec{q}|} kT m_b^2 \exp\left(\frac{\mu_b - e_-}{kT}\right) \,, \tag{31}$$

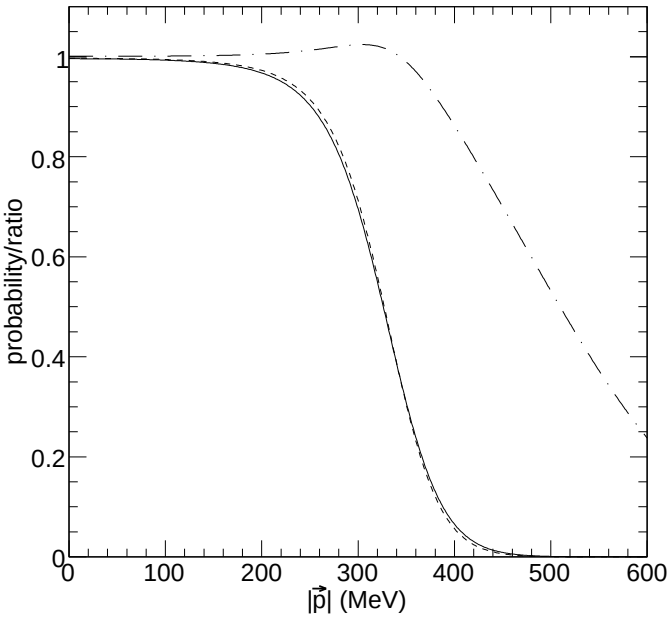

FIG. 3: Comparison between a relativistic (F_R, solid line) and a non-relativistic Fermi distribution (F_{NR}, dashed line), for $kT = 10$ MeV and $n = 0.16$ fm^{-3}. The dash-dotted line represents the ratio F_{NR}/F_R.

with,

$$e_- = \frac{1}{4}\frac{(\omega - |\vec{q}|^2/2m_b)^2}{|\vec{q}|^2/2m_b}. \tag{32}$$

The main difference between the relativistic and non-relativistic expressions for $S(\omega, |\vec{q}|)$ in the classical limit, is the dependence on kT and T_-, and the presence of a term proportional to ω in the relativistic formulation. It can be shown that Eq. (31) is valid when $|\vec{q}| \ll 2m_b$ and $\omega \approx 0$. For $|\vec{q}| \ll 2m_b$ and finite values of ω, a correction given by the $(m_b + kT + T_-)^2$ is essential. When $|\vec{q}| \ll 2m_b$ is not valid anymore, the second correction $\omega(m_b + kT + T_-)$ starts playing an important role. The term $(kT)^2$ only becomes important at higher temperatures.

D. Cross sections

The differences between relativistic and non-relativistic calculations of the dynamical form factor translate themselves in the corresponding cross sections. Therefore, we studied the influence of a relativistic treatment of the Fermi function on the cross sections and the neutrino mean free path $\lambda = \frac{1}{n\sigma}$. Fig. 5 shows the difference in mean free path between our relativistic and the non-relativistic calculation of Ref. [6], for neutral and charged-current processes. It is clear that relativistic calculations predict larger cross sections and a smaller mean free path for the neutrinos.

Figs. 6 and 7 illustrate another interesting feature of the neutrino-nucleon processes. The weak magnetic contribution in the current operator, which was earlier shown to play a substantial role, induces some asymmetry for the polarization of the final nucleon. Figures 6 and 7 display the separated spin contributions to the cross sections as a function of the incoming neutrino energy and energy exchange. Cross sections are shown for both polarization directions of the final nucleon. Thereby, the spin quantization axis is along the direction of the impinging neutrino. The cross section for a final nucleon with $S = -\frac{1}{2}$ is considerably larger than the one for $S = +\frac{1}{2}$.

Polarization effects were shown to be large in neutrino-induced nucleon knockout reactions from nuclei [16, 17, 18]. Apparently, similar mechanisms govern the spin dependence of neutrino interactions in nuclear matter. The polarization effects might be of importance under circumstances of strong magnetic fields. In Ref. [19], a study of the neutrino-nucleon interactions in a strong magnetic field is presented. Thereby, the weak magnetic term responsible for sizable spin-polarization asymmetries, has been neglected.

The strong suppression of charged-current reactions at low incoming neutrino energies, is mainly due to the Pauli blocking of the outgoing electrons. This is seen in the top left panel of Fig. 7 for $kT = 5$ MeV. The CC cross section is smaller by several orders of magnitude than the NC one. For a hadron gas at low temperatures in beta equilibrium, the chemical potential is about 60 MeV for a density of 0.16 fm^{-3}. As a consequence, low energetic neutrinos are not able to create an electron which is not blocked. Fig. 7 shows clearly that the charged-current channel is the most important one at higher energies. For a neutrino energy of 150 MeV, the chemical potential is 114 MeV. Higher temperatures make the Fermi distribution shift to higher energies, an effect further enhancing the charged-current cross sections.

Summarizing, we studied neutrino interactions in a relativistic Fermi gas. Our results for neutrino scattering on a single nucleon are in excellent agreement with previous calculations. In the limit of low temperatures and vanishing nucleon chemical potential, our cross-section calculations coincide with those for scattering on a single nucleon. We find important differences in neutrino cross sections and the neutrino mean free path between relativistic and non-relativistic calculations. In a relativistic treatment, neutrino cross sections are larger. We have shown that the weak magnetic contribution in the weak current is responsible for considerable asymmetries in the polarization of the scattered nucleons. In future work, the correlations will be implemented.

Acknowledgments

The authors wish to thank H.-T. Janka for interesting discussions. They are grateful to the Fund for Scientific

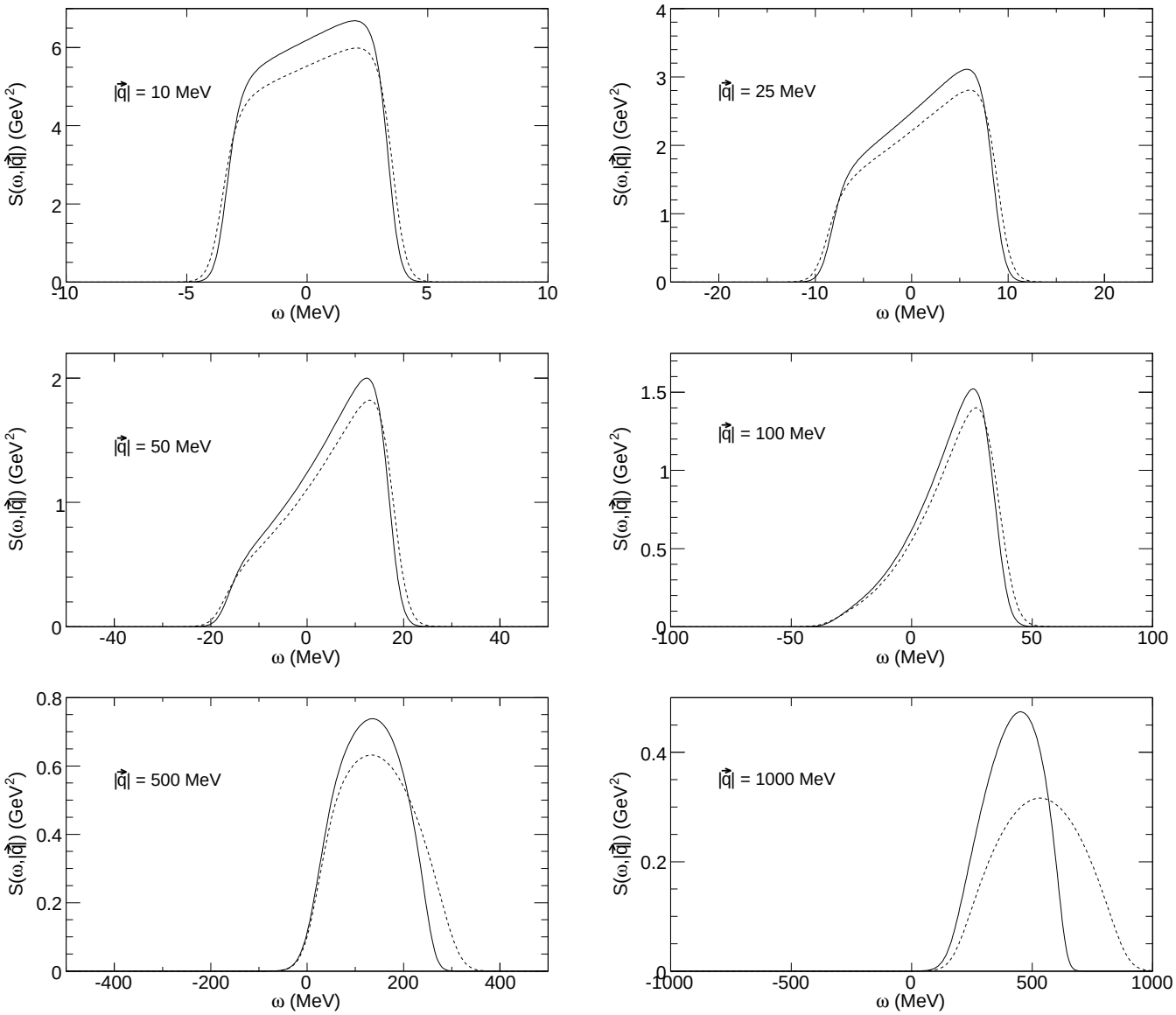

FIG. 4: The dynamical form factor $S(\omega, |\vec{q}|)$ for a neutron gas with density $n = 0.16$ fm^{-3} at a temperature of $kT = 10$ MeV, for various values of the momentum transfer. The solid line represents the relativistic calculation, the dashed line the non-relativistic one.

Research (FWO) Flanders and the UGent University Research Board for financial support.

[1] R. Buras, M. Rampp, H. T. Janka, and K. Kifonidis, Phys. Rev. Lett. **90**, 241101 (2003).

[2] D. L. Tubbs and D. N. Schramm, Astrophys. J. **201**, 467 (1975).

[3] P. Schinder, Astrophys. J. Suppl. Ser. **74**, 249 (1990).

[4] A. Burrows and J. M. Lattimer, Astrophys. J. **307**, 178 (1986).

[5] S. W. Bruenn, Astrophys. J. Suppl. **58**, 771 (1985).

[6] S. Reddy, M. Prakash, and J. M. Lattimer, Phys. Rev. D **58**, 013009 (1998).

[7] A. Burrows and R. F. Sawyer, Phys. Rev. C **58**, 554 (1998).

[8] C. J. Horowitz and K. Wehrberger, Nucl. Phys. **A531**, 665 (1991).

[9] P. Vogel, Phys. Rev. D **29**, 1918 (1984).

[10] C. J. Horowitz, M. A. Pérez-García, and J. Piekarewicz, Phys. Rev. C **69**, 045804 (2004).

[11] G. Watanabe, K. Sato, K. Yasuoka, and T. Ebisuzaki, Phys. Rev. C **68**, 035806 (2003).

[12] S. Cowell and V. R. Phandharipande, Phys. Rev. C **73**,

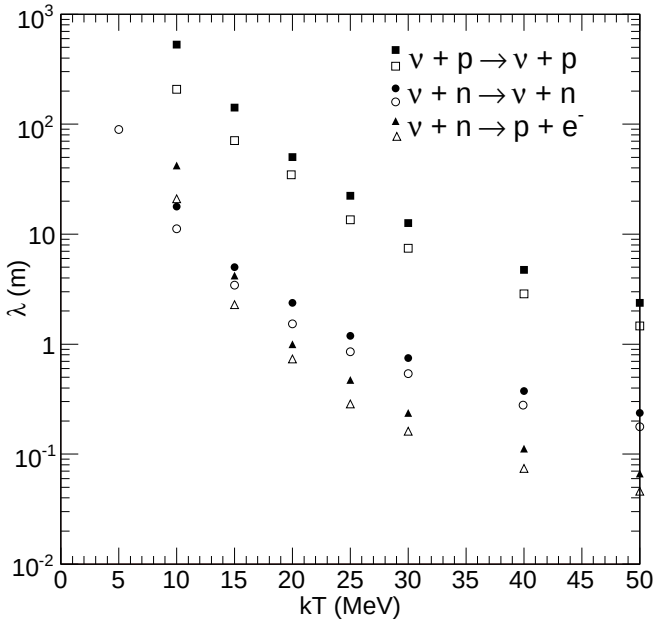

FIG. 5: Neutrino mean free path as a function of the temperature for a nucleon gas in beta equilibrium with $\mu_\nu = 0$ and $n = 0.16$ fm^{-3}. All results are for an initial neutrino energy of $3kT$. The open markers present results of our relativistic calculation and are compared to the non-relativistic results of Ref. [6] (filled markers). The squares represent the mean free path for neutral-current scattering off protons ($\nu + p \to \nu + p$), circles for neutral-current interactions with neutrons ($\nu + n \to \nu + n$), and the triangles for the charged-current neutrino-interaction ($\nu + n \to p + e^-$).

025801 (2006).
[13] G. Watanabe and H. Sonoda (2005), cond-mat/0502515.
[14] J. Bernstein, *Elementary Particles and Their Currents* (W. H. Freeman and Company, 1968).
[15] M. Grypeos, C. Koutroulos, V. Lukyanov, and A. Shebeko, J. Phys. **G24**, 1913 (1998).
[16] N. Jachowicz, K. Vantournhout, J. Ryckebusch, and K. Heyde, Phys. Rev. Lett. **93**, 082501 (2004).
[17] N. Jachowicz, K. Vantournhout, J. Ryckebusch, and K. Heyde, Phys. Rev. C **71**, 034604 (2005).
[18] P. Lava, N. Jachowicz, M. C. Martínez, and J. Ryckebusch, Phys. Rev. C **73**, 064605 (2006).
[19] H. Duan and Y.-Z. Qian, Phys. Rev. D **72**, 023005 (2005).

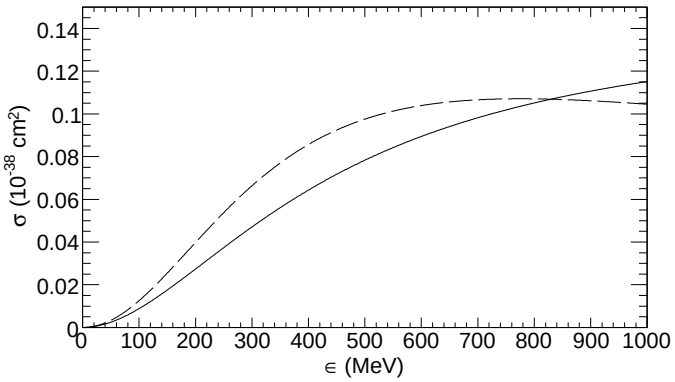

FIG. 6: Polarization of the outgoing nucleon for neutral-current scattering off a neutron. The spin-quantization axis is defined parallel with the direction of the incoming neutrino. The full (dashed) line represents the contribution for final nucleons with spin-up (spin-down) to the cross sections.

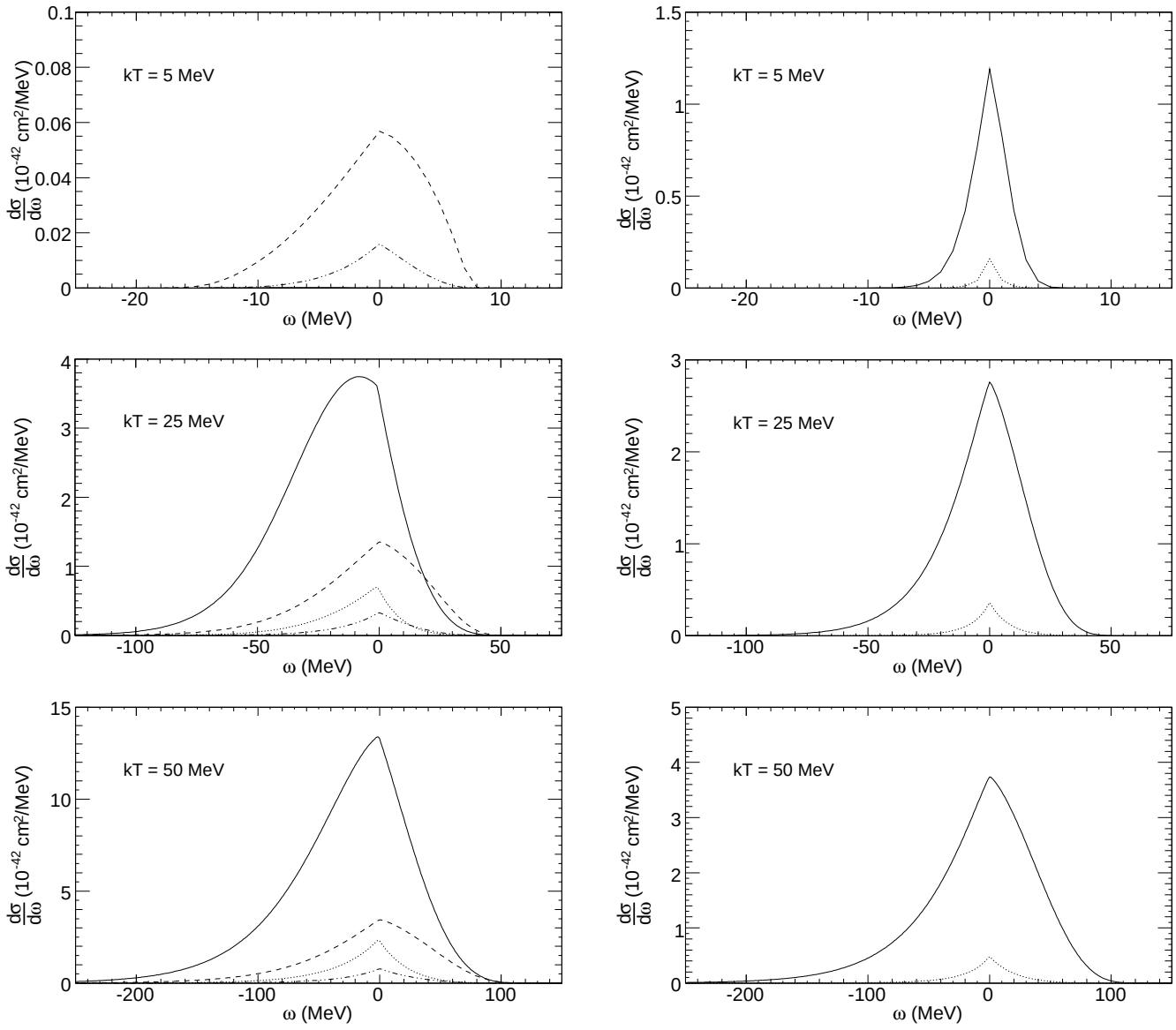

FIG. 7: Different polarization contributions to the differential cross section for neutrino scattering in neutron matter with a density $n_B = 0.16$ fm^{-3} and temperatures $kT = 5,\ 25,\ 50$ MeV. The incoming neutrino energy is $3kT$. The left panels present neutron cross sections: CC with final spin down (solid line) ; CC with final spin up (dotted) ; NC with final spin down (dashed) ; NC with final spin up (dashed-dotted). The right panels are for neutrino-proton scattering : NC with final spin down (solid line) and NC with final spin up (dotted). The quantization axis for the spin of the outgoing nucleon was chosen parallel to the incoming neutrino's momentum.